Optimal design of a four-sensor probe system to measure the flow properties of the dispersed phase in bubbly air-water multiphase flows.

PRADHAN, S.R., MISHRA, R., UBBI, K. and ASIM, T.

2013

Optimal design of a four-sensor probe system to measure the flow properties of the dispersed phase in bubbly air-water multiphase flows

S. R. Pradhan[1], R. Mishra[1], K. Ubbi[1], T. Asim[1]

s.r.pradhan@hud.ac.uk ; r.mishra@hud.ac.uk ; k.s.ubbi@hud.ac.uk ; T.Asim@hud.ac.uk

[1] University of Huddersfield, Queensgate, Huddersfield, HD1 3DH

Abstract

This paper presents a systematic investigation on the design and development of a four-sensor probe system to be used for air-water multiphase flow measurements. A mathematical model is presented which can be used to determine the optimum axial separation of the front sensor with respect to three rear sensors within a four sensor probe system. This system can be used to measure flow properties of the dispersed phase in bubbly air-water flows accurately. Paper also presents a sensitivity analysis to determine the minimum sampling frequency requirements in the data collection process, so that associated errors in various output parameters can be minimized, for the given values of sensors co-ordinates. A particularly novel feature of this paper is development of a unique digital signal processing scheme to enable the accurate computation of different flow characteristics.

This paper also presents validation of four- sensor probe measurements from a flow visualization and measurement system which relies on using two high speed cameras mounted orthogonally. The results obtained from validation experiments show very high degree of similarity in measured flow variables from the two systems. This indicates that the four-sensor probe system developed in this study can be used with confidence to measure parameters of a dispersed multiphase flow. The flow characteristics obtained from the four-sensor probe system when used in a multiphase flow system are also presented. The results indicate a unique flow pattern corresponding to bubbles of different sizes in air-water flows.

Keywords: bubbly multiphase flow, four-sensor probe, velocity vector, gas volume fraction, bubble diameter, time delay

Nomenclature

i, j, k	Unit vectors in x, y and z direction (probe coordinate system(m))
N	Number of bubble striking sensor
$\hat{n}_i$	The unit vector in the direction of **r**
$\hat{n}_v$	The unit vector in the direction of **V**

$\mathbf{r}$	Position vector of point of first contact of bubble with sensor 0(m)
r	Magnitude of $\mathbf{r}$ (m)
$\mathbf{r_1}$	Position vector of point of first contact of bubble with sensor 1(m)
r_1	Magnitude of $\mathbf{r}$ (m)
S	Axial distance between the front and the rear sensor (m)
T	Sampling time (s)
U_g	Superficial velocities of gas (m/s)
U_w	Superficial velocities of water (m/s)
$\mathbf{V}$	Velocity vector
V_{amp}	Output voltage from op amp (V)
V_{in}	Circuit input voltage (V)
V_{out}	Circuit output voltage (V)
v	Velocity magnitude (m/s)
v_r	Radial velocity or the velocity at the Y-axis (m/s)
v_z	Axial velocity or the velocity at the z-axis (m/s)
v_θ	Azimuthal velocity or the velocity at the X-axis (m/s)
x, y, z	Probe Coordinate (m)
x_1, x_2, x_3	x coordinates of sensor 1, 2 and 3 with respect to sensor 0 (m)
y_1, y_2, y_3	y coordinates of sensor 1, 2 and 3 with respect to sensor 0 (m)
z_1, z_2, z_3	z coordinates of sensor 1, 2 and 3 with respect to sensor 0 (m)
α	Polar angle (^{0})
β	Azimuthal angle (0)
δt_{0a}	Time delays equal to zero (s)

δt_{0a} Time taken for bubble to cross the sensor 0 (s)

δt_{1a} δt_{1b} Time delay between first bubble contact with the sensor 0 and first and last bubble contacts respectively with sensor 1(s)

δt_{2a} δt_{2b} Time delay between first bubble contact with the sensor 0 and first and last bubble contacts respectively with sensor 2(s)

1 Introduction

Multiphase flows are fairly common in many chemical, mining and mechanical industries. Air-water flows are typical of multiphase flows where density difference between the dispersed phase and the continuous phase is quite large. The essential parameters in two-phase air-water bubbly flows include volume fraction distribution of the dispersed phase, interfacial area concentration and the bubble size distribution corresponding to the dispersed phase.

Conductivity probes are used widely to measure various flow characteristics of bubbly multiphase flows within pipelines [1-15]. Wu et al [16] have shown that a dual-sensor probe can be used to measure the time averaged velocity and interfacial area concentration of the dispersed phase in air-water multiphase flows with reasonable accuracy. However dual-sensor probes, because of their very nature, can only estimate the axial bubble velocity. Hence the use of dual-sensor probes for measuring dispersed phase parameters in three dimensional multiphase flows is not recommended. This challenge was overcome by introduction of a four-sensor probe to enable measurements of velocity vector (magnitude and direction) of the dispersed phase in bubbly multiphase flows [1-2]. Mishra et al [1] and Lucas et al [2] have presented a theoretical model which is used to compute various flow properties corresponding to the dispersed phase in typical bubbly air-water flows using the time delay measurements from a four-sensor probe. The developed model is based on the following assumptions:-

1. The Mathematical model is valid for spherical bubbles.
2. The impact of a bubble on the probe does not affect the bubble's velocity vector.
3. Bubbles do not get deformed during the process of interaction with sensors.

Figure 1 shows a schematic diagram of a typical four-sensor probe and the motion of a bubble of radius R moving with velocity vector **V.** The velocity vector can be represented mathematically as:-

$$\boldsymbol{V} = \boldsymbol{v}(sin\alpha sin\beta \mathbf{i} + sin\,\alpha\,cos\beta \mathbf{j} + cos\,\alpha\,\mathbf{k}) \tag{1}$$

where v is velocity magnitude, α is polar angle between velocity vector and probe axis and β is an azimuthal angle for velocity vector. Lucas et al [2] developed a detailed procedure to calculate polar angle α and azimuthal angle β of vertically rising bubble from time delay measurements made by the four-sensor probe. The corresponding equations are given below.

$$\tan\beta = \frac{\left(\frac{z_1}{\delta t_{11}} - \frac{z_2}{\delta t_{22}}\right)\left(\frac{y_1}{\delta t_{11}} - \frac{y_3}{\delta t_{33}}\right) - \left(\frac{z_1}{\delta t_{11}} - \frac{z_3}{\delta t_{33}}\right)\left(\frac{y_1}{\delta t_{11}} - \frac{y_2}{\delta t_{22}}\right)}{\left(\frac{z_1}{\delta t_{11}} - \frac{z_2}{\delta t_{22}}\right)\left(\frac{x_1}{\delta t_{11}} - \frac{x_2}{\delta t_{22}}\right) - \left(\frac{z_1}{\delta t_{11}} - \frac{z_2}{\delta t_{22}}\right)\left(\frac{x_1}{\delta t_{11}} - \frac{x_3}{\delta t_{33}}\right)} \tag{2}$$

$$\tan\alpha = \frac{\left(\frac{z_1}{\delta t_{11}} - \frac{z_2}{\delta t_{22}}\right)}{\left(\frac{x_1}{\delta t_{11}} - \frac{x_2}{\delta t_{22}}\right)\sin\beta - \left(\frac{y_1}{\delta t_{11}} - \frac{y_2}{\delta t_{22}}\right)\cos\beta} \tag{3}$$

$$\frac{v\delta t_{ii}}{2} = x_i \sin\alpha\sin\beta + y_i \sin\alpha\cos\beta + z_i \cos\alpha \tag{4}$$

Velocity magnitude v can be calculated using equation 4, where δt_{ii} represents the time interval between the contacts of the front sensor and i^{th} rear sensor with the bubble, x_i, y_i and z_i are coordinate of ith rear sensor with respect to front sensors. Mishra et al. [8] later extended this model to compute other parameters of interest i.e. D, μ and ϑ, where D is diameter of a bubble, μ is the polar angle corresponding to the point of contact of front sensor and ϑ is the azimuthal angle corresponding to the point of first contact of the front sensor as defined in figure 1C. Various geometric parameters corresponding to bubble size and the first point of contact on a bubble have been shown in figure 1C. The relevant equations are shown below.

$$\tan\vartheta = \frac{\left(\frac{z_1}{A_{11}} - \frac{z_3}{A_{33}}\right)\left(\frac{y_1}{A_{11}} - \frac{y_2}{A_{22}}\right) - \left(\frac{z_1}{A_{11}} - \frac{z_2}{A_{22}}\right)\left(\frac{y_1}{A_{11}} - \frac{y_3}{A_{33}}\right)}{\left(\frac{z_1}{A_{11}} - \frac{z_2}{A_{22}}\right)\left(\frac{x_1}{A_{11}} - \frac{x_3}{A_{33}}\right) - \left(\frac{z_1}{A_{11}} - \frac{z_3}{\delta t_{33}}\right)\left(\frac{x_1}{A_{11}} - \frac{x_2}{A_{22}}\right)} \tag{5}$$

$$\tan\mu = \frac{\left(\frac{z_2}{A_{22}} - \frac{z_1}{A_{11}}\right)}{\left(\frac{x_1}{A_{11}} - \frac{x_2}{A_{22}}\right)\sin\vartheta - \left(\frac{y_1}{A_{11}} - \frac{y_2}{A_{22}}\right)\cos\vartheta} \tag{6}$$

Diameter of a bubble D can be calculated using equation 7, where $i = 1, 2$ and 3

$$\frac{A_{ii}}{D} = \sin\mu\sin\vartheta + \sin\mu\cos\vartheta + \cos\vartheta \tag{7}$$

Thus, using the above equations, most of the flow parameters corresponding to the dispersed phase in air-water multiphase flows can be measured. Above model shows that for accurate measurement of dispersed flow parameters, time delays must be measured accurately. The accurate measurement of the time delays can be affected by location of four sensors in a four probe system. Hence for accurate measurement of flow parameters of the dispersed phase, for a given flow condition, a four-sensor probe needs to have an optimum sensors configuration.

Wu et al. [16] investigated the effect of axial sensors' separation on accuracy of velocity measurement for spherical and elliptical bubbles in air-water flow using typical dual-sensor probes. Authors concluded that measurable velocity may approach infinity if the ratio of the sensors' separation to the diameter of measured bubbles was smaller than the maximum relative fluctuation of the bubble velocity. Wu et al. [16] therefore suggested using an axial sensors' separation which is greater than half of the bubble diameter for effective elimination of this singularity problem.

Corre et al. [17] suggested a non-dimensional sensor separation parameter (axial separation divided by bubble diameter) in the range of 0.6 to 1 for accurate velocity measurements. The above recommendations were based on numerical simulations and hence effects of all the parameters have not been explicitly included in the probe design. The criteria proposed, also do not take into account likely flow conditions. This paper presents the development of an analytical model to determine the sensors locations for accurate measurement of dispersed phase flow parameters in a wide variety of multiphase flow conditions. In addition this paper explores possible circuits and presents a novel digital signal processing scheme to maximize the accuracy of measurements using the four sensor probe system.

2 An analytical model for placement of sensor in a four sensor probe system

Section 1 shows that the equations 2, 3, 4, 5, 6 and 7 can be used to calculate various parameters defining the velocity vector of any moving bubble (polar angle α, azimuthal angle β, velocity magnitude v) and various parameters defining bubble size (polar angle corresponding to the point of first contact μ, azimuthal angle corresponding to the point of first contact ϑ and the diameter of a bubble D) of any moving air bubble in an air-water flow field. In these equations the input parameters are the time delays and the ith sensor's co-ordinates $x_i, y_i,$ and z_i. The time delay values are obtained from the bubbles' signatures recorded at various sensors using appropriate circuit and digital signal processing scheme. Figure 2 shows an ideal signal output from a typical four-sensor probe during its interaction with a bubble. Lucas et al [2] have shown that the time delays corresponding to the motion of a bubble from the leading sensor to the ith rear sensor δt_{ia} and δt_{ib} (first and second contacts) can be calculated using following equations: -

$$\delta t_{ia} = \frac{-b - \sqrt{(b^2 - 4ac)}}{2a} \tag{8}$$

$$\delta t_{ib} = \frac{-b + \sqrt{(b^2 - 4ac)}}{2a} \tag{9}$$

Where

$$a = v^2$$

$$b = -v\{2r\,\hat{n}_v\hat{n}_i + 2x_i\hat{n}_v.\mathbf{i} + 2y_i\hat{n}_v.\mathbf{j} + 2z_i\hat{n}_v.\mathbf{k}\}$$

$$c = \{x_i^2 + y_i^2 + z_i^2 + 2\,r\,x_i\,\hat{n}_i\,.\mathbf{i} + 2\,r\,y_i\,\hat{n}_i\,.\mathbf{j} + 2\,r\,z_i\hat{n}_i.\mathbf{k} + r^2 - r^2\}$$

In order to ensure that a bubble hits all four sensors, it is important that $(b^2 - 4ac)$ is always positive. In multiphase flow situations, it is essential that probes are designed in such a way that probes record signatures of most of the bubbles flowing through the point of interrogation. An in-adequately designed probe may result in the measurement of non-representative flow parameter values which may seriously affect the accuracy. Therefore, in this section a mathematical model is developed so that the maximum permissible value of axial separation z_i can be estimated that will ensure that most of the moving bubbles touch all sensors of a four-sensor probe. The mathematical model allows determination of maximum permissible z_i for all rear sensors based on pre-defined coordinates x_i and y_i of

corresponding rear sensors. The maximum permissible z_i value therefore must satisfy following equation.

$$b^2 = 4\,ac \tag{10}$$

Where,

$\rightarrow\ b^2 = (-v\{2r\,\hat{n}_v\hat{n}_i + 2x_i\hat{n}_v.\mathbf{i} + 2y_i\hat{n}_v.\mathbf{j} + 2z_i\hat{n}_v.\mathbf{k}\})^2$

$\rightarrow\ 4\,ac = 4\,v^2(x_i^2 + y_i^2 + z_i^2 + 2\,r\,x_i\,\hat{n}_i\,.\mathbf{i} + 2\,r\,y_i\,\hat{n}_i\,.\mathbf{j} + 2\,r\,z_i\hat{n}_i.\mathbf{k})$

$\rightarrow\ (\{(r\,\hat{n}_v\hat{n}_i + x_i\hat{n}_v.\mathbf{i} + y_i\hat{n}_v.\mathbf{j}) + z_i\hat{n}_v.\mathbf{k}\}^2) = (x_i^2 + y_i^2 + z_i^2 + 2\,r\,x_i\,\hat{n}_i\,.\mathbf{i} + 2\,r\,y_i\,\hat{n}_i\,.\mathbf{j} + 2\,r\,z_i\hat{n}_i.\mathbf{k})$

Let $t = 2r\,\hat{n}_v\hat{n}_i + 2x_i\hat{n}_v.\mathbf{i} + 2y_i\hat{n}_v.\mathbf{j}$

Therefore

$(\{t + z_i\cos\alpha\}^2) = (x_i^2 + y_i^2 + z_i^2 + 2\,r\,x_i\sin\mu\sin\vartheta + 2\,r\,y_i\,\sin\mu\cos\vartheta + 2\,r\,z_i\cos\mu)$

$\rightarrow\ t^2 + 2z_i\cos\alpha\,t + (z_i\cos\alpha)^2 = (x_i^2 + y_i^2 + z_i^2 + 2\,r\,x_i\sin\mu\sin\vartheta + 2\,r\,y_i\,\sin\mu\cos\vartheta + 2\,r\,z_i\cos\mu)$

$\rightarrow\ t^2 - (x_i^2 + y_i^2 + Dx_i\sin\mu\sin\vartheta + D\,y_i\,\sin\mu\cos\vartheta) = 2z_i\cos\alpha\,t - z_i^2 + (z_i\cos\alpha)^2 + (2\,r\,z_i\cos\mu)$

$t = 2r(\sin\alpha\sin\beta\sin\mu\sin\vartheta + \sin\alpha\cos\beta\sin\mu\cos\vartheta + \cos\alpha\cos\mu) + 2x_i\sin\alpha\sin\beta + 2y_i in\,\alpha\,\cos\beta$

$\rightarrow z_i\ (2\cos\alpha\,t + D\cos\mu) + z_i^2(1 - \cos^2\alpha) - \langle t^2 - (x_i^2 + y_i^2 + Dx_i\sin\mu\sin\vartheta + D\,y_i\,\sin\mu\cos\vartheta)\rangle = 0 \tag{11}$

The solutions of above equation can be written as:-

$$z_i = \frac{-n \mp \sqrt{(n^2 - 4mo)}}{2\,m} \tag{12}$$

Where

$m = (1 - \cos^2\alpha)$

$n = (2\cos\alpha\,t + D\cos\mu)$

$o = -\langle t^2 - (x_i^2 + y_i^2 + Dx_i\sin\mu\sin\vartheta + D\,y_i\,\sin\mu\cos\vartheta)\rangle$

The solution to equation 12 yields one positive value of z_i, which is used in this analysis. From the above equation the value of z_i can be computed for given values of v, α, β, μ, ϑ, and D. Thus if an estimate of likely flow conditions is available a probe can be designed for

measurements with greater accuracy for those specific flow conditions. In the following section, a parametric study has been presented that shows the dependence of the maximum permissible axial separation of sensors on different types of flow conditions.

2.1 Calculation of maximum z_i required of the various values of v_x, v_y and v_z

In practice, the flow characteristics of the dispersed phase in multiphase flows may vary from one dimensional to strongly three dimensional and prior information about likely flow field may be used to design a four-sensor probe for a specific requirement. To establish this interdependence, an investigation has been carried out to establish relationship between the required axial separation of the sensors and the flow field characteristics. Different flow conditions were simulated by varying magnitudes of v_x and v_y with respect to v_z. Here v_x, v_y and v_z are x, y and z components of the resultant velocity. The main flow is assumed to be in the z direction. For this parametric investigation v_x and v_y were varied within a range of 0.01% (approximately one dimensional flow) of v_z to 100% of v_z (Strongly three dimensional flow) for different sizes of bubbles (2mm-15mm) moving across a probe. Values of velocity magnitude v and angles μ and ϑ were kept constant and chosen as follows, v = 1 m/s, μ = 15°, ϑ = 45°. Probe dimensions used in these investigations are as shown in table 1. These dimensions correspond to three different frontal areas of the probe, which are 0.25 mm^2, 0.5 mm^2 and 0.75 mm^2.

Figure 3A shows the maximum permissible z_i for various flow conditions ranging from strongly one dimensional to strongly three dimensional for a probe with frontal area 0.5 mm^2. It can be clearly seen that required z_i decreases as flow changes from one dimensional to three dimensional. Hence for highly three dimensional flows maximum permissible axial separation is smaller as compared to primarily axial flows. For a typical bubble of 5 mm the required z_i decreases by about half. However, values of z_i increase as diameter of bubble increases, as bigger bubbles have higher likelihood of touching all the sensors even with larger axial separation. Previous work from Corre et al. [17] suggested this value to be in between 0.6 to 1 times the diameter. It can be clearly seen that such an axial separation is completely unsuitable for strongly three dimensional flows and there is a need to establish a relationship between the axial separation of sensors and the likely flow for which that separation will be adequate which figure 3A provides.
The frontal area of a probe has large influence on axial separation of sensors as well. To establish this, simulations were carried out on probes with three different frontal areas.

Figure 3B shows the comparison of maximum permissible z_i for three different fontal areas, 0.25mm^2, 0.5 mm^2 and 0.75 mm^2, for $v_x = 0.1v_z$, $0.6\ v_z$ and $1v_z$. It can be seen that for a probe with larger frontal maximum axial separation should be smaller as compared to probe with smaller frontal area. This is because for a probe with larger frontal area there is a less likelihood of all the sensors being touched by a bubble. Hence probes with smaller frontal area are preferred for such measurement. Furthermore, a probe with smaller frontal area offers less resistance to the on-coming bubble as well. Comparing above three results it can be concluded that as the frontal area increases, maximum permissible z_i required decreases. Overall it can be concluded that maximum permissible z_i is more for one dimensional flows and larger bubble diameter. Results also establish that figure 3A and 3B can be used as design charts in addition to equation 12 to determine axial separation of the rear sensors with respect to the front sensor as a function of flow conditions for accurate measurement.

2.2 Sensitivity analysis

The requirements of smaller frontal area and small axial separation needed for accurate measurements put more emphasis on the accuracy of time delay measurements. Since the bubbles are expected to move with reasonably high velocity across the sensors, time delay measurements need to be extremely accurate for accurate estimation of the dispersed phase parameters. In order to measure the dispersed phase parameters accurately, it is necessary to acquire a reliable and representative signal from each sensor. Figure 4 shows the ideal output of a typical dual-sensor probe. If data is sampled at a frequency (fs) with a dual-sensor probe, the time interval (Δt) between two time signals is given by Equation 13.

$$\Delta t = \frac{1}{fs} \tag{13}$$

Actual local gas velocity v_{true} can be computed using equation 14.

$$v_{true} = \frac{s}{\delta t_1} \tag{14}$$

δt_1 is measured time delay and "s" is axial probe separation.

Depending on accuracy of time measurements the measured time delay can be in the range of δt_1 to $\delta t_1 \pm \dfrac{1}{fs}$

Hence, the accuracy of measured local gas velocity v_{meas} will depend on value of sampling frequency as shown in equation 15.

$$v_{meas} = \frac{s}{\delta t_1 \pm \dfrac{1}{fs}} \tag{15}$$

Therefore, as sampling frequency increases the difference between v_{true} and v_{meas} tends towards zero. For a four-sensor probe, it is not easy to predict the interrelation between various flow parameters and sampling rate. Hence in this section a sensitivity analysis has been carried out in order to determine the reasonable sampling frequency needed for accurate time delay measurements. Accuracy in measurement of α, β, v, μ, ϑ and D depends on accuracy in measurement of seven time delays (δt_{0b}, δt_{1a}, δt_{1b}, δt_{2a}, δt_{2b} δt_{3a} and δt_{3b}). The accuracy of measurement of time delays in turn depends on sampling rate. To quantify the effect of sampling rate, it was assumed that bubbles of 5mm diameter were moving across a four sensor probe, with dimension as shown in the table 1 (with 0.5mm^2 frontal area). It was also assumed that a typical bubble was flowing with a velocity magnitude of 1ms^{-1}. Although there are a number of possible flow conditions, in the present investigation values of β, μ and ϑ are chosen as 45°. The analysis was carried out for various polar angles ranging from 0° to 35° degrees.

Various error values were then introduced in the range of $1e^{-7}$ to $1e^{-4}$ in the true time delays values to simulate the effects of sampling frequency limitations of data acquisition on measured values of the time delays. The errors were introduced in such a way that for each value of α there are 128 possible combinations of errors as shown in table 2. In table 2, 'e' is assumed error. To quantify effects of time delays errors on flow parameters, average percentage errors and average absolute percentage errors have been computed as shown below.

Assume $V_{\kappa i(cal)}$ is calculated parameter of bubble where $\boldsymbol{\kappa}$ can be any of the x, y and z (for velocity components) with i^{th} combination of error and $V_{\boldsymbol{\kappa}}$ is its true value. Therefore, for i^{th} combination, error $\boldsymbol{\epsilon}_i$ in the measurement of a particular parameter can be defined as:-

$$\epsilon_{\kappa i} = \left(\frac{V_{\kappa i(cal)} - V_\kappa}{V_\kappa}\right) 100\% \qquad (16)$$

For given value of V and for given value of e, an average percentage error $\bar{\boldsymbol{\epsilon}}$ can be defined as

$$\bar{\varepsilon}_\kappa = \frac{1}{128}\sum_{i=1}^{128}\epsilon_{\kappa i} \qquad (17)$$

An average absolute percentage error $\bar{\varepsilon}_{\kappa(abs)}$ can be defined as

$$\bar{\varepsilon}_{\kappa(abs)} = \frac{1}{128}\sum_{i=1}^{128}|\epsilon_{\kappa i}| \qquad (18)$$

Figure 5A shows the percentage error $\bar{\varepsilon}_z$ in the calculated values of axial velocity magnitude for different values of e and for various polar angles in the range of 5° to 35°. It can be seen that as error e increases the error values in calculated velocity magnitudes tend to increase as well. The figure shows that the error in calculated velocity magnitudes increases significantly when error e is more than $1e^{-5}$.

Figure 5B shows the percentage error $\bar{\varepsilon}_y$ in the calculated values of y component of the velocity for different values of e and different values of polar angle in the range of 5° to 35°. It can be seen, that as the error e increases the error in calculated y component velocity tends to increase as well, as seen earlier in figure 5A. Again when error e is more than $1e^{-5}$ the error in y component velocity magnitudes becomes higher.

Figure 5C shows the percentage error $\bar{\varepsilon}_x$ in calculated values of x-component of velocity for different values of e and polar angles in the range 5°- 35°. It can be seen that values of $\bar{\varepsilon}_x$ starts to increase rapidly when error e becomes more than $1e^{-5}$. The above clearly indicates that the data acquisition must be carried out at a rate 10^5 samples per second to limit inaccuracies in measurement of velocity components.

Calculations have also been carried out to determine absolute percentage error in calculated values of V_x, V_y and V_z. Figures 6 (A), (B) and (C) show the absolute average percentage error in calculated values of velocity components V_x, V_y and V_z respectively for different values of error as discussed earlier. It can be seen from figure 6 (A) that $\bar{\varepsilon}_{x(abs)}$ values are relatively small for e values up to $1e^{-5}$s. $\bar{\varepsilon}_{x(abs)}$ values however, increase sharply as e increases beyond $1e^{-5}$s . For a value of e equals to $1e^{-4}$, $\bar{\varepsilon}_{x(abs)}$ is approximately 120% for α =

5°, where as it is about 70% for α = 10°. These values of $\bar{\varepsilon}_{x(abs)}$ are relatively large for small values of α, i.e. where V_x is very small. The reason for this is that although the error in calculated velocity components is relatively small, they still represent a relatively large proportion of actual velocity component. A similar variation in average absolute percentage error $\bar{\varepsilon}_{y(abs)}$ with e and α can be observed in figure 6(B).

The variation of an average absolute percentage error $\bar{\varepsilon}_{z(abs)}$ for different values of e is shown in figure 6 (C). The maximum value $\bar{\varepsilon}_{z(abs)}$ of is less than 2% for e equals to $1e^{-5}$s and increases to 10% for e equals to $1e^{-4}$s.

The above results suggest that V_x V_y and V_z can be measured within 2% of accuracy, provided the seven time delays $\delta t_{0b}, \delta t_{1a}, \delta t_{1b}, \delta t_{2a}, \delta t_{2b}, \delta t_{3a}, \delta t_{3b}$, are made within an accuracy of 10μs. It is however recommended, that the time delay measurements should be made with an accuracy of 1μs for very accurate results.

2.3 Construction of the four-sensor probe

Earlier sections have very clearly highlighted the requirements imposed on the design of a four-sensor probe system for the measurement of dispersed phase parameters in a multiphase flow. For a moderately three dimensional flow ($V_x = V_y = 0.5\ V_z$), based on the above findings a four-sensor probe was constructed. Such a probe should work well for primarily axial flows as well as for moderately three dimensional flows. For constructing the probe, Teflon (PTFE) coated needles of 0.15mm in outer diameter were used as sensor of the probe. All four sensors of the probes have been placed in such a way that they make an isosceles triangle where front sensor lies in the center of this triangle. This layout also increases the probability of bubbles making the contact with the lead sensor first and then with the rear sensors. In order to achieve this layout a centrally drilled 2mm diameter ceramic guide was used to mount the needles. This also helps in minimising the overall frontal area of the probe. Design of this probe is shown schematically in figure 7. The stainless steel tube forming the probe body was used as common earth electrode for the four sensors.

2.4 Circuit and Signal Processing

In a typical four sensor probe, the probe body and each of four sensors act as a negative and positive electrode respectively of a close circuit and are designed to have a pre-defined voltage. The change in voltage level depends on whether sensor is in contact with water phase or gas phase. To measure the voltages corresponding to bubble motion across each set of electrodes a circuit as shown in figure 8 was designed to record the bubble signature signals similar to that shown in figure 2. Figure 8 shows a simulated signal generated using non-inverting amplifier. Using this circuit it is opssible to generate an output which is almost inversally proportional to the probe resistance. Identical circuits were built and used to measure the voltage across electrodes of each sensor. The input and output quantities available from the non-inverting circuit can be mathematically represented by the following equation.

$$V_a = V_{in} \left(1 + R_{ref}/R_s\right)$$

(19)

In equation 19, R_s is the resistance between the tip of a relevant sensor and stainless steel tube forming probe body. When the tip of a given sensor is immersed in water, with respect to figure 8, R_s is relatively small compared to R_{ref} (which has a typical value of 1-1.5M) thus, V_a saturates at positive supply voltage. When the tip of needle is immersed in an air bubble, the quantity R_{ref} is relatively small as compare to R_s making V_a approximately equal to V_{in}. Thus, as each sensor is alternately immersed in water and air, output signals similar to those shown in figure 9 are obtained.

From figure 9 it can be seen that, although the identical circuits were made, the signals from four different sensors are not identical. This can be due to the various factors such as tolerance level of the resistors used and exposed area of the sensor tip itself. Hence the following signal processing scheme was developed to extract required information from probe signals.

1. The output signals from the four-sensor conductivity probe differ from an ideal square-wave, hence, proper threshold voltage values are needed to generate accurate time intervals δt_{ii}.
2. The bubble-probe interaction is complex because some bubbles only touch some of the four sensors and it is necessary to find out which of the four 'square-wave' signals are caused by the same bubble.
3. In any flow condition, not all the bubbles unambiguously contact each sensor twice, leading to errors in the estimates of δt_{ii}. Consequently, such bubbles should be ignored in order to improve the accuracy of the calculation.
4. For accuracy of the calculation, the signals with small voltage drop (less than 0.1 times average voltage drop) as well as the signals with small residence time (0.1 times average residence time) are ignored.

The threshold voltage ((v_{th}) see figure 10) was used to determine the rising and the falling edge of the signals achieved from the four-sensor probe. These correspond with arrival and departure of a bubble at the sensor tip. The level of threshold can change the residence time of a given sensor in a bubble, which is given by equation 20; where δt_i residence is time of ith sensor in bubble, δt_{if} and δt_{ir} is first and last contact of a bubble by i^{th} sensor respectively. Thus accurate estimate of threshold is necessary for accurate estimation of flow parameters. In previous experiments [13], the threshold values were arbitrarily chosen (v_{th1} in figure 10) to ensure the threshold values are beyond the noise in signals achieved from four-sensor probe. This value may not necessarily represent actual arrival and departure time of the bubble at a sensor and hence a suitable strategy needs to be developed to compute threshold from the data available.

$$\delta t_i = \delta t_{ir} - \delta t_{if} \tag{20}$$

In order to overcome this uncertainty, a process of identifying the threshold voltage was developed. This process ensures that at a point of measurement in the flow field, law of conservation of mass is satisfied. As per this constraint, all the sensors within a four sensor probe must give same volume fraction of the dispersed phase. This process will ensure that all the sensors satisfy mass conservation constraint at all the points in the flow field. The developed system implements an iteration process with different threshold values and calculates the volume fraction [see equation 21] of the dispersed phase from each sensor. The calculated volume fraction was then compared with the reference volume fraction measured

using D.P cell as described by Pradhan et al. [13]. The individual threshold voltage for each sensor was chosen when the calculated volume fraction is equal to reference volume fraction or the difference between calculated and reference volume fraction is less than 0.0001.

$$\text{Volume fraction } \varepsilon = \frac{1}{T}\sum_{n=1}^{N}(\delta t_i)_n \tag{21}$$

Figure 11 shows calculated volume fraction for all four sensors before and after iteration process. The results indicate that, the calculated volume fraction from each sensor can be matched with the reference volume fraction (.02459). Results also indicate that threshold voltage for each sensor can be of different values. Thus a novel digital signal processing scheme has been developed which accurately estimates the level of threshold needed for each sensor in a four sensor system. This ensures that time delay values in the calculation of different parameters correspond to actual motion of bubble across the sensors.

3 Validation of the four sensor probe measurement system

To test the accuracy of a four-sensor probe measurement system, controlled tests were carried out using two independent measuring systems as explained below.

3.1 Comparisons of probe and camera systems

Initially, bench test experiments were carried out. These experiments were carried out in a tank of dimensions 300mm x 300 mm x 800 mm. Table 3 represents the probe dimensions that were used to collect the data. In this test, it was expected that the bubbles moving across the probes would have mean diameter of about 5 mm and that the flow would be primarily axial. Hence, the axial separation of rear sensors from the leading sensor was kept at 1.75 mm, 1.83 mm and 1.91 mm respectively.

In order to validate the results obtained by the four-sensor probe system, a system that includes two high speed cameras was introduced. These cameras were placed orthogonally as shown in figure 12. Both the cameras were capable of capturing the pictures of a moving object simultaneously at a speed of 250 frames per second. Since the primary motive behind using high speed cameras was to compare the velocity vectors calculated by the probe with the velocity vectors calculated by the camera system, it was essential that the data collected by four-sensor probe was from same bubble as that captured by cameras.

In order to ensure that both cameras capture the same bubble that strikes all four sensors of the probe, a mid-trigger system was used to capture images from both cameras, as well as to record signals from the four sensor probe as described by Pradhan et al [13]. The captured images were processed and the velocity and diameter of the bubbles were calculated as described by Pradhan et al [13]. The calculated bubble diameter and velocity obtained from the cameras were then compared with the results obtained using the four-sensor probe system. Figure 13 shows a comparison of the diameters of the bubbles as determined from the four-sensor probe system and as captured by the camera system. The figure shows that there is an excellent match in the diameters of the calculated bubbles using both probe and the camera systems. The average percentage error in the calculated diameters from the two systems is found to be 2.92%. Table 4 shows a comparison of velocity magnitudes calculated using the four-sensor probe system and camera system. It clearly shows that the average difference in velocity values obtained from probe and camera systems is only 2.51%.

The above results shows that a four sensor probe system can be used to measure dispersed phase parameters with good accuracy. To test the usability of four probe sensor systems in practical situation, multiphase flow loop tests were carried out. In the following, results obtained from use of a four-sensor probe system in a typical multiphase flow loop have been presented.

3.2 Flow loop experiments

Following the promising results from bench test, the four-sensor probe system was used in a flow loop in order to measure the velocity components (azimuthal velocity, redial velocity, axial velocity), the volume fraction and the diameter of the bubbles passing through different points in a pipe cross section. The flow loop is designed to create different types of flow and it was decided to test four-sensor probe in primarily axial as well as highly three dimensional flows. For this purpose, the experiments were carried out with and without the presence of a swirler in a vertical pipeline of 80 mm diameter. The swirler consisted of six brass vanes which were welded to a central brass hub measuring 10mm in diameter and was set at 20°. Design of the four-sensor probe for this application required simulation of motion of bubbles of different sizes across the probe. It was decided to keep frontal area of the probe as small as possible. The typical probe used has the co-ordinates as shown in Table 5.

Figure 14 shows the results from analytical model for maximum permissible axial separation for such a probe. It can be seen that for 6 mm bubble the axial separation needed is about 2 mm for primarily axial flow. For a typical three dimensional flow with $V_x=V_y=0.4\ V_z$, a maximum permissible axial separation of 1.5 mm is ok. Hence in the present investigation the axial separation used satisfies the criteria adopted.

Two different flow conditions [a) $U_w = 0.76m/s$, $U_g = 0.04m/s$ b) $U_w = 0.57m/s$, $U_g = 0.02m/s$] were used where U_w represents superficial water velocity and U_g represents superficial gas velocity. For each flow condition, the probe was used at six radial locations on each given pipe radius to obtain the data. The pipe section containing the probe was rotated 30° anti-clockwise to take data along to the next radius. The same process was repeated for twelve different radii to collect the data at a total of 61 different locations, as shown in Figure 15.

Figures 16 shows the variation of polar angle α with r/D with and without the presence of the swirler for U_g= 0.02 ms^{-1} and U_w= 0.57ms^{-1} and U_g= 0.04ms^{-1} and U_w= 0.76ms^{-1}. From the figure it can be seen that the swirler causes noticeable effect on the polar angle for tested values of air and water superficial velocities. It also shows that the polar angle increases very little (but is noticeable) as the flow rate increases. Figure also indicates that at the pipe center bubble primarily move vertically up where as nearer the wall they may velocity vectors which make an angle of about 20^0 with the pipe axis.

Figures 17 shows the variation of velocity magnitude with non-dimensional radial position r/D with and without presence of swirler for U_g= 0.02 ms^{-1} and U_w= 0.57ms^{-1} and U_g= 0.04ms^{-1} and U_w= 0.76ms^{-1}. From the figure it can be seen that swirler has very little effect (but is noticeable) on the shape of the velocity magnitude for tested values of air and water superficial velocities. However it is also evident that velocity magnitude increases as the flow rate increases. Figure also indicates that the velocity is much lower at the wall of pipe at lower flow conditions.

Figures 18 shows the variation of azimuthal velocity v_θ with r/D with and without the presence of swirler for test conditions $U_w = 0.57\text{ms}^{-1}$ and $U_g = 0.02$ ms^{-1} and $U_w = 0.76\text{ms}^{-1}$ $U_g = 0.04\text{ms}^{-1}$. It is clear from the above the azimuthal velocity v_θ is relatively close to zero at all positions in the flow cross section for non-swirler flows. However, at $U_w = 0.76\text{ms}^{-1}$ $U_g = 0.04\text{ms}^{-1}$ flow rate, the presence of the swirler causes the azimuthal velocity v_θ to be strongly negative close to the pipe walls.

Figures 19 shows the variation of polar angle μ with r/D, for the test conditions $U_w = 0.57\text{ms}^{-1}$ and $U_g = 0.02$ ms^{-1} and $U_w = 0.76\text{ms}^{-1}$ $U_g = 0.04\text{ms}^{-1}$. It is clear that when U_w is equal to 0.57 m/s, the presence of the swirler has a small effect on the polar angle μ across the pipe section as compared to the flow when U_w is equal to 0.76 m /s. The presence of the swirler also shows a larger effect on the profile of polar angle μ. Figure also indicates that when the probe is at the center of pipe, probe touches bubbles at the center. However, as the probe moves towards the wall of pipe, probe touches the bubbles at a point away from the center.

Figures 20 shows the variation of polar angle ϑ with non-dimensional radial position r/D, for the test conditions $U_w = 0.57\text{ms}^{-1}$ and $U_g = 0.02$ ms^{-1} and $U_w = 0.76\text{ms}^{-1}$ $U_g = 0.04\text{ms}^{-1}$. From the figure it can be seen that without the presence of swirler there is very small change on the azimuthal angle corresponding to point of first contact as the flow was increased. Figure also indicates that azimuthal angle corresponding to point of first contact remains almost same when the probe is moved across the pipe in both flow conditions. However the presence of swirler makes the azimuthal angle ϑ changed rapidly as the probe is moved from center to the pipe wall.

Figures 21 shows the variation of diameter of bubble with r/D, for the test conditions $U_w = 0.57\text{ms}^{-1}$ and $U_g = 0.02$ ms^{-1} and $U_w = 0.76\text{ms}^{-1}$ $U_g = 0.04\text{ms}^{-1}$. Results show that there is a very small but noticeable variation on the bubble diameter measured under both flow conditions. Results also suggest that there is very small effect in the measurement of the bubble diameter due to the presence of the swirler which is expected.

The above results indicate that a four-sensor probe can be used with confidence to measure dispersed phase flow parameters with confidence in multiphase applications. Furthermore axial separation of sensors can be tuned to acquire better measurements in such applications.

4 Conclusions

An analytical model for the optimization of probe spacing has been developed for specified flow conditions. It enables calculation of maximum permissible axial separation of sensors for a four-sensor probe for various flow conditions. The results clearly show that the required maximum z_i decreases as the flow changes from one dimensional to three dimensional. However, values of z_i increases as the diameter of bubble increases. The study shows that a probe with larger frontal area will have less possibility of all the sensors being touched by a bubble. Thus, a probe with smaller frontal area is more suitable for measurement of the time delays in air-water bubbly flow.

Sensitivity analysis for the probe dimensions indicated that for the accurate measurement of time delays from the sensor, data should be collected at minimum $1e^5$ Hz, but preferably

at $1e^6$ Hz. A novel digital signal processing scheme was developed that relies on threshold levels required to match the calculated volume fraction with the reference volume fraction. For validation purpose bench test results were compared with results from high speed cameras and the flow parameter values obtained from the two systems matched very closely.

Flow loop experiments were carried out with and without the presence of swirler for various ranges of flow conditions. Results show that the presence of swirler shows significant increase in the azimuthal velocity. The results also show that at the center of the pipe section probe tends to touch the bubble at its center however as the probe moves towards the pipe wall it touches bubble at the edge of the bubble making the polar angle larger.

The study shows that four-sensor can be used to measure the flow properties of the bubble flowing in air-water bubbly flow. The errors can be minimized if data are collected using carefully designed probe and sampled at $1e^5$ Hz or above.

References

[1] R. Mishra, G. P. Lucas, H. Kieckhoefer, A model for obtaining the velocity vectors of spherical droplets in multiphase flows from measurements using an orthogonal four-sensor probe, Meas. Sci. Tech. 13 (2002) 1488-1498.

[2] G. P. Lucas, R. Mishra, Measurement of bubble velocity components in a swirling gas-liquid pipe flow using a local four-sensor conductance probe, Meas. Sci. Tech.16 (2004) 749-758.

[3] N. Panagiotopoulos, G. Lucas, Simulation of a local four-sensor conductance probe using a rotating dual-sensor probe. Meas. Sci. Tech. 18 (2007) 2563-2569.

[4] S. Pradhan, G. Lucas, N. Panagiotopoulos, Sensitivity Analysis for a 4-SensorProbe Used for Bubble Velocity Vector Measurement Researchers conference University of Huddersfield 2006.

[5] S. Hosgett, M. Ishii, Local two-phase flow measurement using sensor techniques, Nuclear engineering and design, 175 (1997) 15-24.

[6] S. Kim, X. Y. Fu, X. Wang X, M. Ishii, Development of the miniaturised four-sensor conductivity probe and the signal processing scheme, International journal of heat and mass transfer, 43 (2000) 4101-4118.

[7] M. Ishii, S. Kim, Micro four-sensor probe measurement of interfacial area transport for bubbly flow in round pipe, Nuclear engineering and design, 205 (2001) 123-131.

[8] R. Mishra, Measurement of volume fraction and bubble velocity in air water flows through a vertical pipe line using a seven sensor probe, Proceedings of the 24th international congress on COMDEM, 30th May – 1st June 2011

[9] G. Lucas, X. Zhao, S. Pradhan, Optimisation of four-sensor probes for measuring bubble velocity components in bubbly air–water and oil–water flows, Flow Measurement and Instrumentation, 22 (2011) 50-63.

[10] Z. Xin, G. Lucas, S. Pradhan, Signal Processing method in using four-sensor probe for measuring the velocity vector of air-liquid two phase flow, Journal of the Japanese Society of Experimental Mechanics (JSEM), 9 (2009) 19-24.

[11] S. Pradhan, G. Lucas, Z. Xin, Measurement of reference velocity vector for four-sensor conductance probes using orthogonal, high speed cameras, 11th International Conference on multiphase flow in industrial plants, (2008) 697-704.

[12] N. Panagiotopoulos, G. Lucas, S. Pradhan, Simulation of a four sensor probe using a rotating dual sensor probe, Proceedings of Computing and Engineering Annual Researchers' Conference (2006) 1-6.

[13] S. Pradhan, Measurement of Bubble Velocity Vectors in Bubbly Air Water Multiphase Flow, Doctoral thesis, University of Huddersfield (2010).

[14] R. Buchholz, J. Steinemann, Application of an electrical conductivity microprobe for the characterization of bubble behaviour in gas-liquid bubble flow, part. Charact, 1 (1984) 102-107.

[15] L.G. Neal and S.G. Bankoff, A high resolution resistivity probe for determination of local void properties in gas–liquid flow, AIChE J.9 4 (1963) 490–494.

[16] Q. wu, K. Welter, D. McCreary, J. N. Reyes, Theoretical studies on the design criteria of double-sensor probe for the measurement of bubble velocity, J. Flow Meas. Instrumentation, 12 (2001) 43-51.

[17] J-M Corre, M. Ishii, Numerical evaluation and correction method for multi-sensor probe measurement technique in two-phase bubbly flow, Nuclear engineering and design, 216 (2002) 221-238.
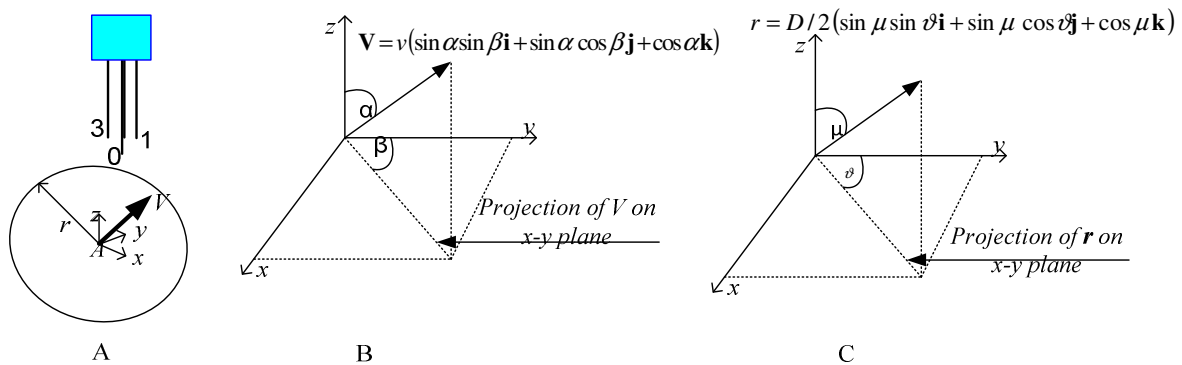
Figure 1 A) Schematic representation of a four-sensor probe B) the droplet and Symbolic representation of velocity vector Mishra et al. [8] C) Symbolic representation of position vector of the point of first contact of droplet with front sensor
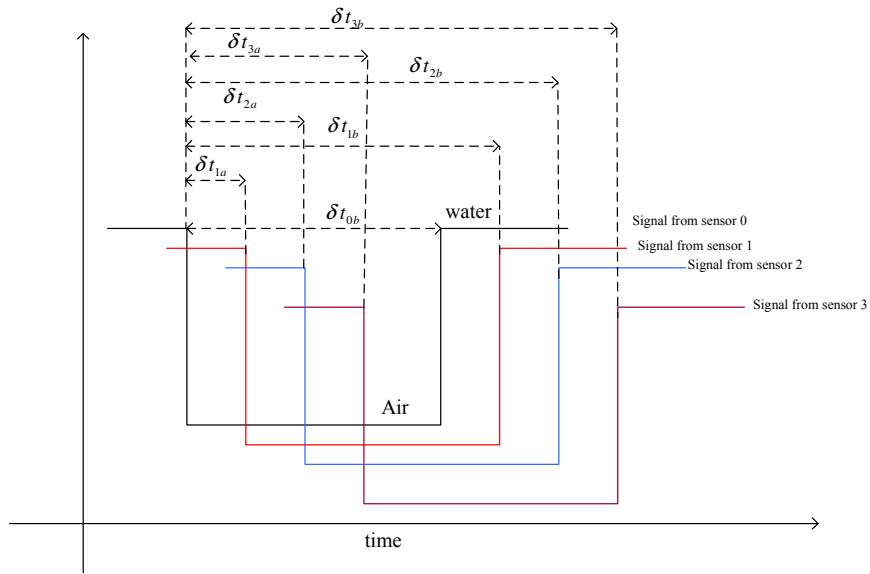
Figure 2 Ideal signals from a four-sensor probe
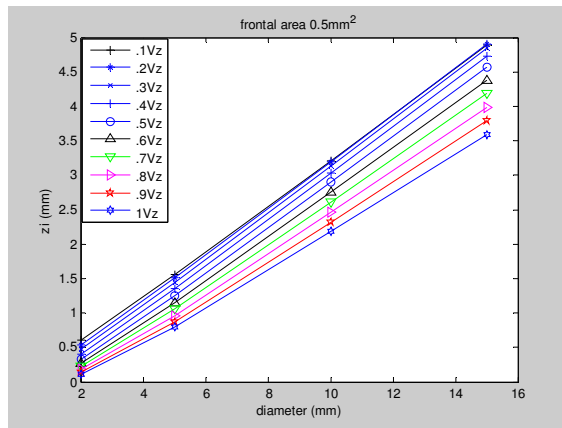
Figure 3A Graphical representation of maximum permissible z_i for probe with frontal area = 0. 5mm^2
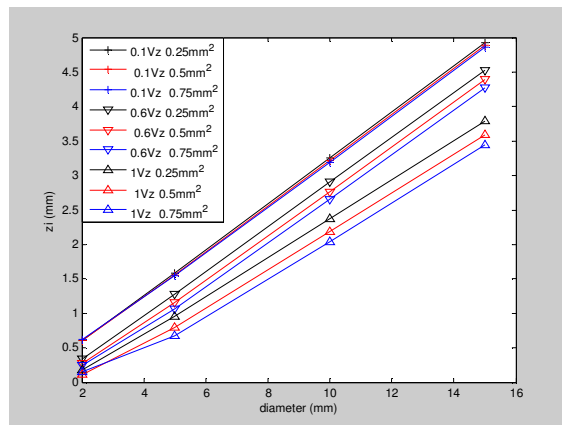
Figure 3B Comparisons of maximum permissible z_i for probe with frontal area = 0.25mm^2, 0.5 mm^2 and 0.75 mm^2 for the given flow conditions
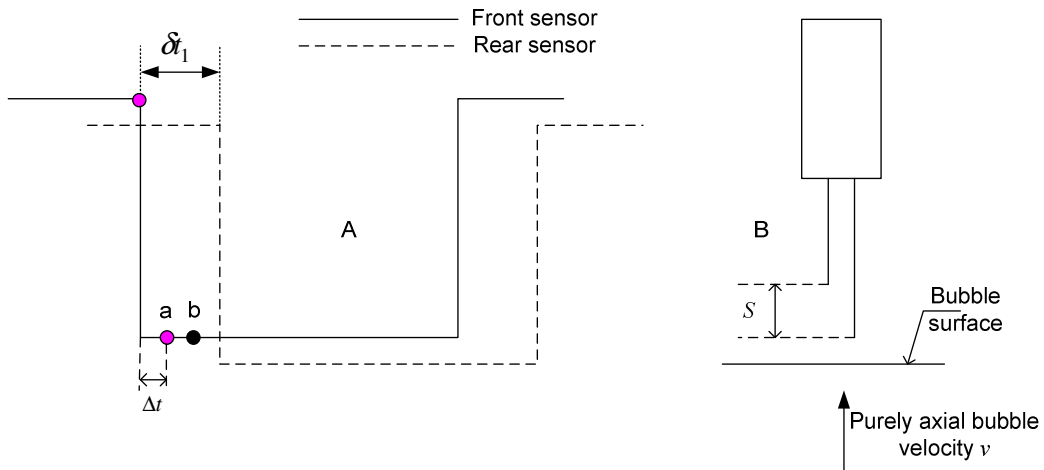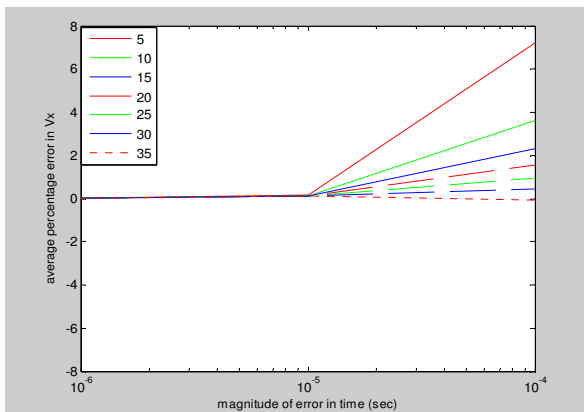
Figure 4 (A) Typical signals from a dual-sensor probe where "a" is the time taken at sampling frequency of 40 KHz and "b" is the time taken at sampling frequency of 20 KHz (B) Dual-sensor probe
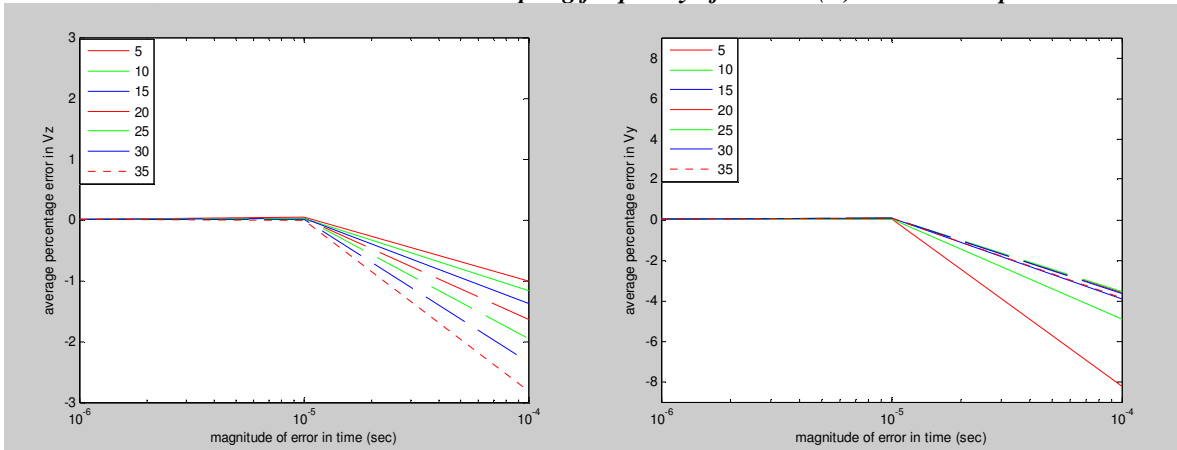
Figure 5A Variations in $\bar{\varepsilon}_z$ with error e for different values of polar angle α

Figure 5B Variations in $\bar{\varepsilon}_y$ with error e for different values of polar angle α

Figure 5C Variations in $\bar{\epsilon}_x$ with error e for different values of polar angle α
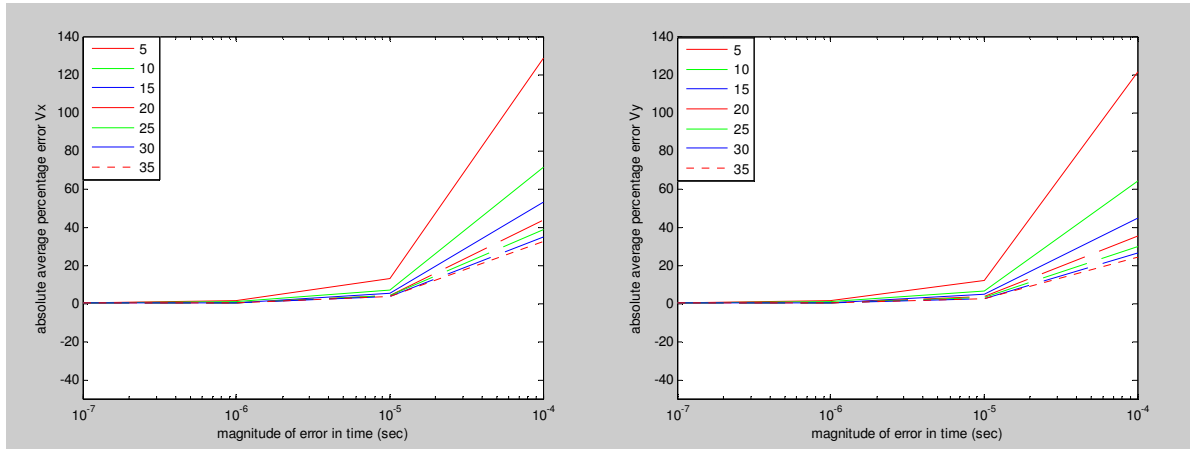
A

B
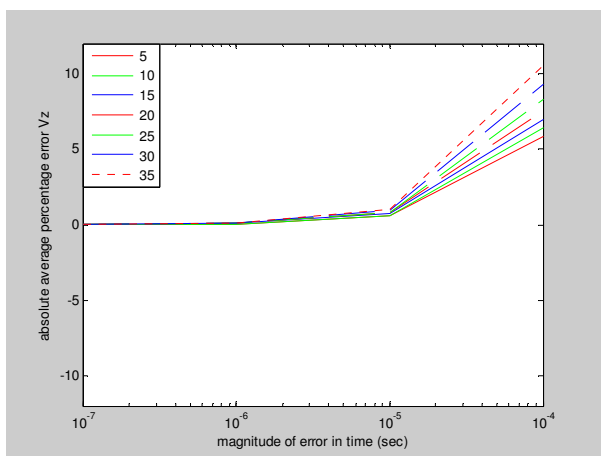
C

Figure 6 Variations in absolute percentage error $\bar{\varepsilon}_x$ (A) $\bar{\varepsilon}_y$(B) and $\bar{\varepsilon}_z$(C) with error e for different values of polar angle α
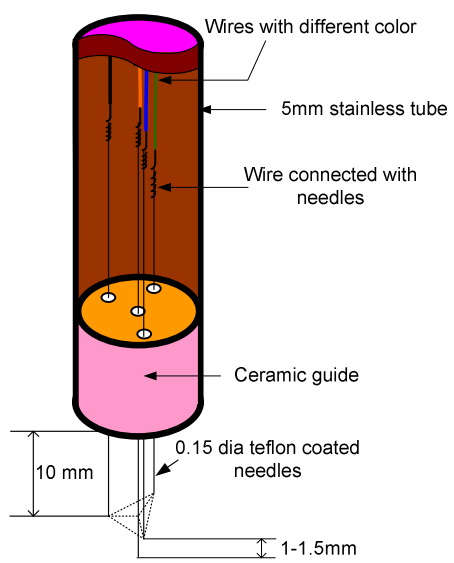
Figure 7 Schematic of four-sensor probe Pradhan et al [13]
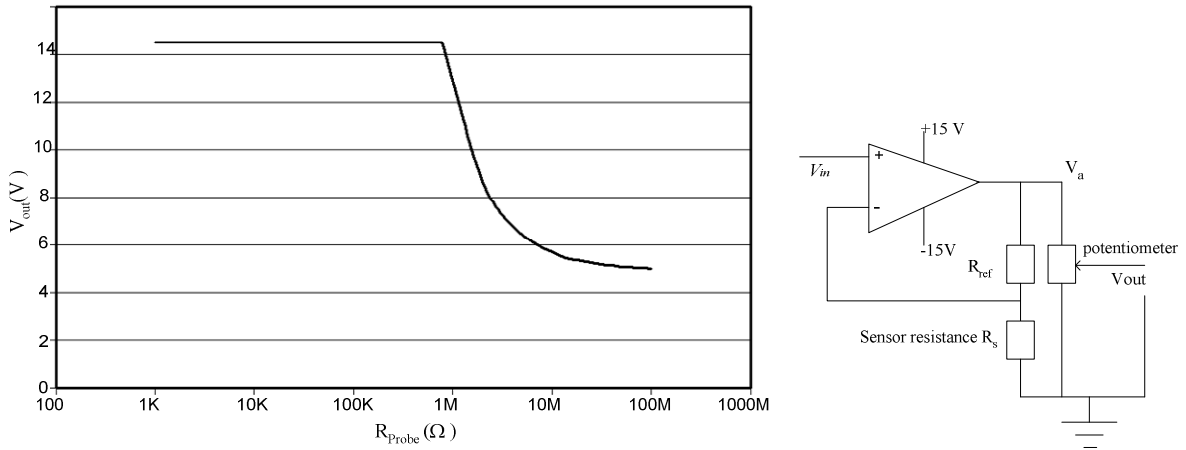
Figure 8 Non inverting amplifier circuit and simulated result
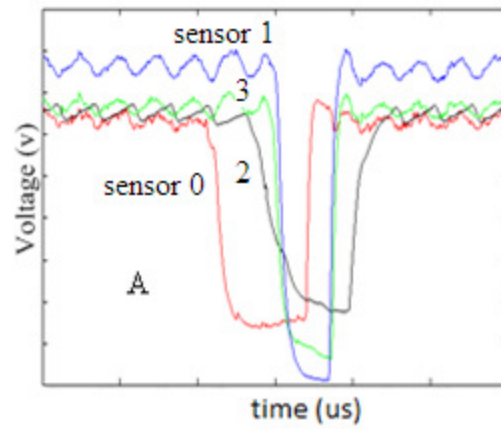
Figure 9 Raw signals from a 4-sensor probe due to the passage of a single gas bubble.
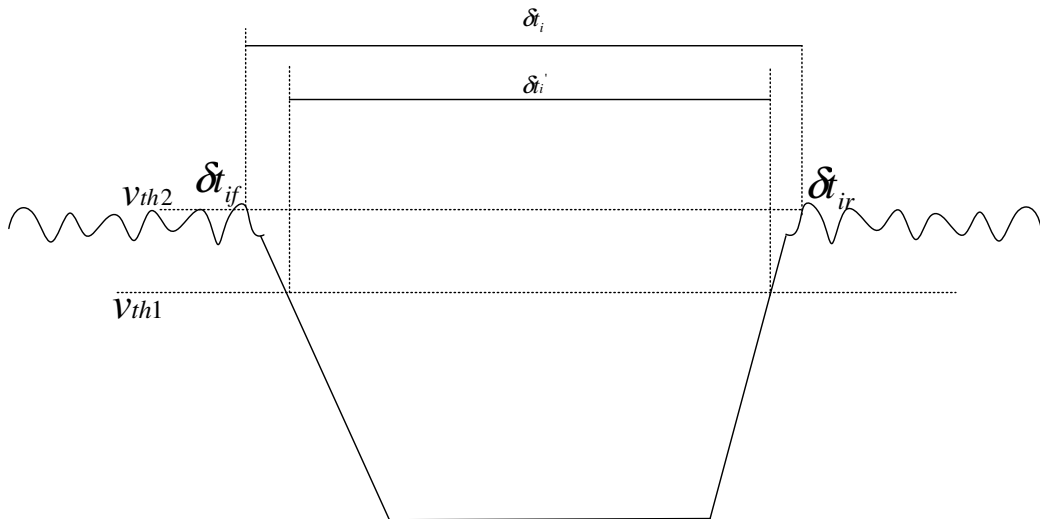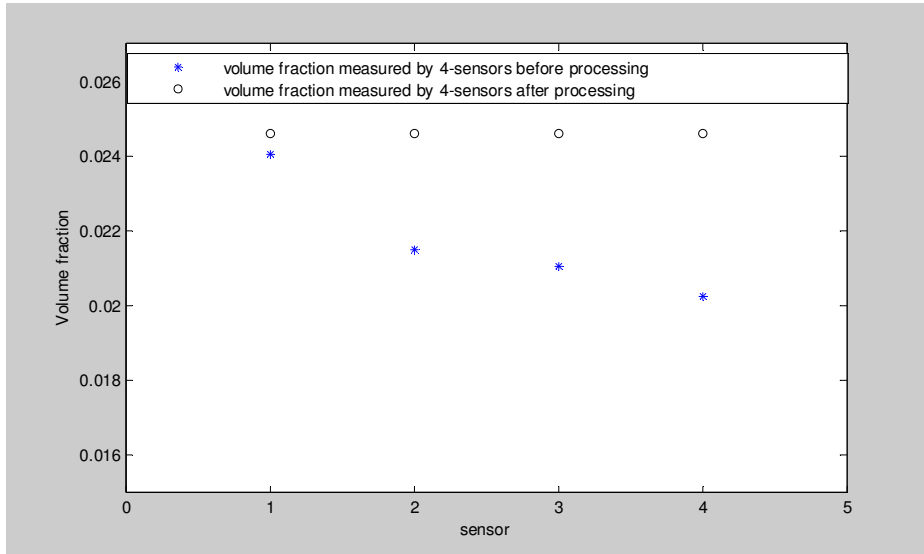

Figure 10 Various threshold levels and residence time of a sensor in a bubble

Figure 11 Volume fraction measured by each sensor before and after threshold iteration process
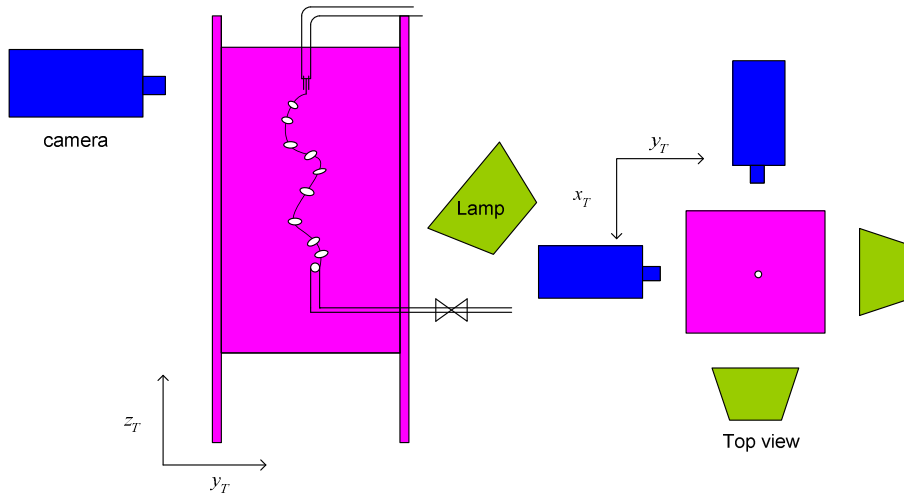
Figure 12 Experimental set up for the tank experiments
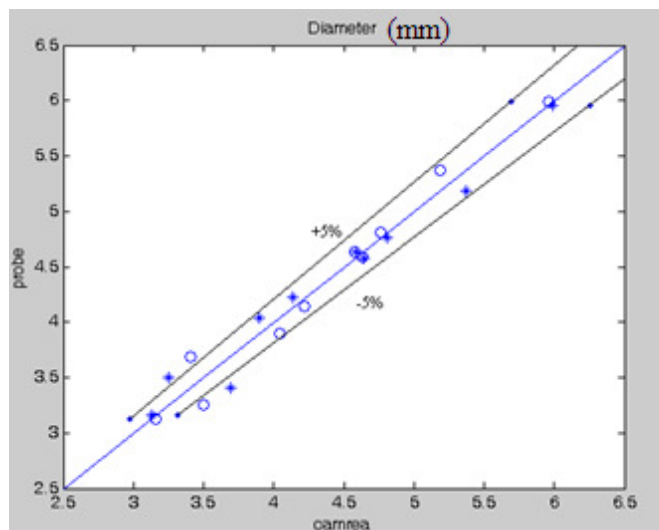
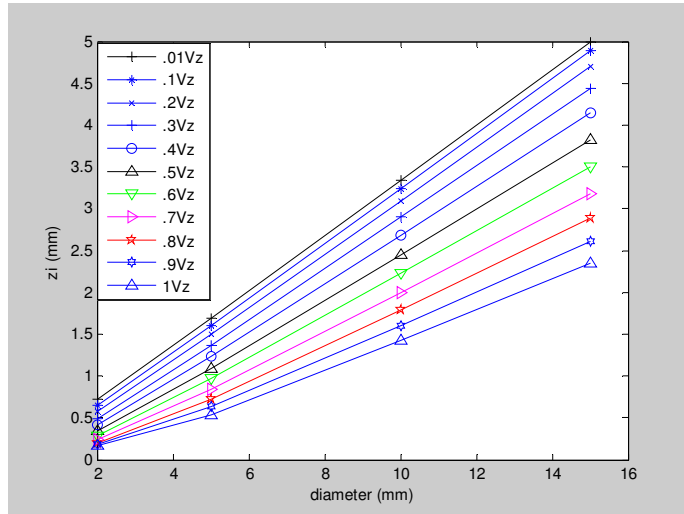*Figure 13 Diameters of the bubbles (in mm) calculated using four-sensor probe and camera*

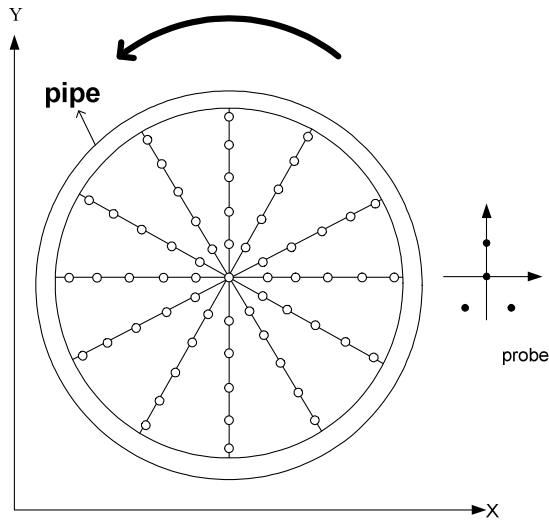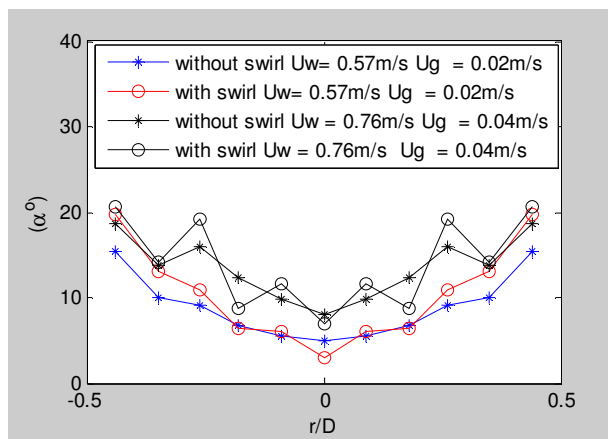*Figure 14 Graphical representation of maximum permissible z_i for actual probe dimensions*
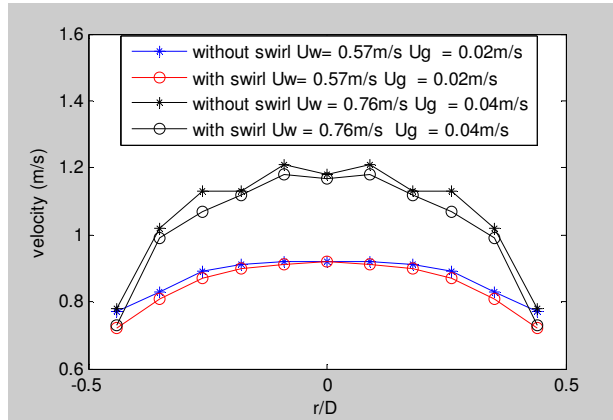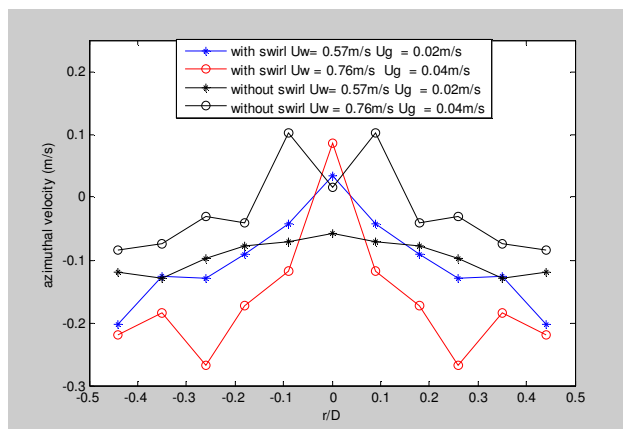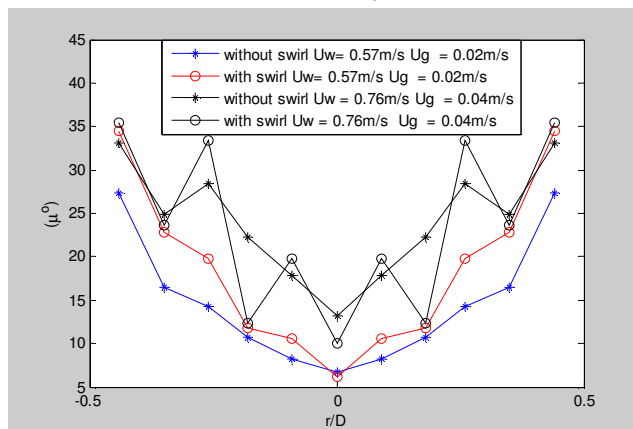

Figure 15 Data collection points in the flow loop

Figures 16 Variation of polar angle versus non-dimensional radial position

Figure 17 Variation of velocity versus non-dimensional radial position

Figures 18 Variation of azimuthal velocity v_θ versus non-dimensional radial position

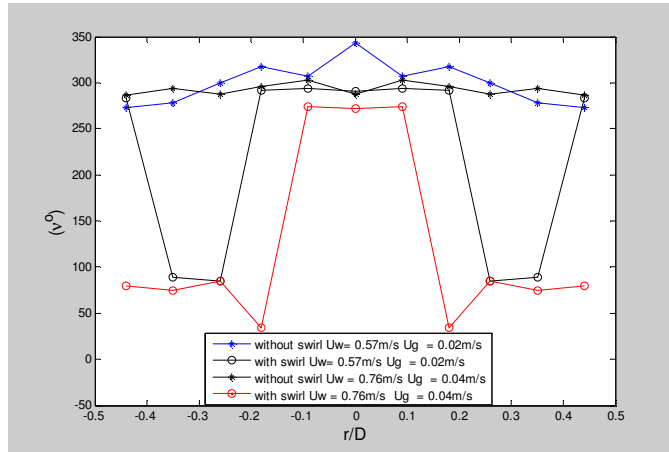*Figures 19 Variation of μ versus non-dimensional radial position*

Figure 20 Variation of ϑ versus non-dimensional radial position

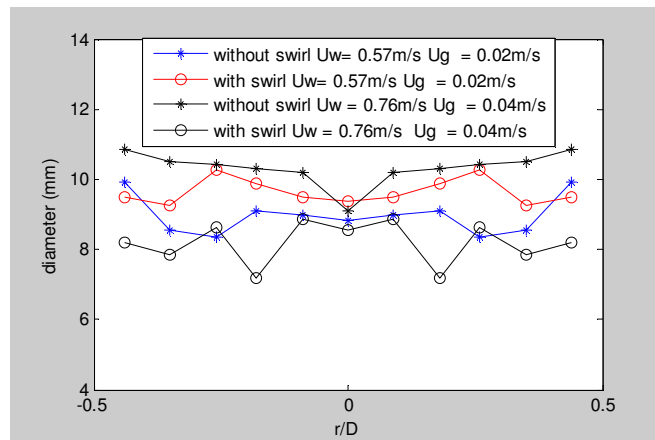*Figure 21 Variation of Diameter versus non-dimensional radial position*

frontal area								
$0.25mm^2$			$0.5mm^2$			$0.75mm^2$		
1	2	3	1	2	3	1	2	3
x	0	0.35	-0.35	0	0.5	-0.5	0	0.61	-0.61
y	0.35	-0.35	-0.35	0.5	-0.5	-0.5	0.52	-0.61	-0.61

Table 1 Probe dimensions used

S/n	assumed values of time delays						
1	$\delta t_{0b}+e$	$\delta t_{1a}+e$	$\delta t_{1b}+e$	$\delta t_{2a}+e$	$\delta t_{2b}+e$	$\delta t_{3a}+e$	$\delta t_{3b}+e$
2	$\delta t_{0b}-e$	$\delta t_{1a}+e$	$\delta t_{1b}+e$	$\delta t_{2a}+e$	$\delta t_{2b}+e$	$\delta t_{3a}+e$	$\delta t_{3b}+e$
3	$\delta t_{0b}+e$	$\delta t_{1a}-e$	$\delta t_{1b}+e$	$\delta t_{2a}+e$	$\delta t_{2b}+e$	$\delta t_{3a}+e$	$\delta t_{3b}+e$
-							
-							
128	$\delta t_{0b}-e$	$\delta t_{1a}-e$	$\delta t_{1b}-e$	$\delta t_{2a}-e$	$\delta t_{2b}-e$	$\delta t_{3a}-e$	$\delta t_{3b}-e$

Table 2 Possible combination of errors in time interval

	1	2	3
x	0.00	0.71	0.57
y	0.57	-0.20	-0.47
z	1.75	1.83	1.91

Table 3 Probe dimensions used for bench test

velocity				
camera	0.38	0.34	0.41	0.35
probe	0.37	0.33	0.38	0.36

Table 4 Calculation of velocity magnitude using probe and camera

	1	2	3
x	0.09	0.44	-0.48
y	0.62	-0.51	-0.34
z	1.51	1.48	1.52

Table 5 Probe dimension used in flow loop experiments

Vitae

Suman Raj Pradhan graduated in Electrical and Electronics engineering with distinction and holds his Ph.D. in instrumentation for multiphase flow from the University of Huddersfield. He was actively involved in Micro-hydro Power development in Nepal and has a keen interest in design and development of sustainable energy. He joined the University of Huddersfield as a Research Assistant in 2011. His research interest includes instrumentation, aero-dynamics, sustainable/renewable energy, multi-phase flow.

Rakesh Mishra holds his Ph.D. in the area of multiphase flow through pipelines from the Indian Institute of Technology, Delhi, India. He is currently a Professor of Fluid Dynamics at the University of Huddersfield, UK. He heads the Energy Emissions and the Environment (E3) research group within the Diagnostics research centre at the University of Huddersfield. He has published more than 150 papers in various journals and conference proceedings.

Kuldip S Ubbi is a senior lecturer in the department of Engineering and Technology within University of Huddersfield, UK. Kuldip has extensive experience in teaching and consultancy in the field of Computer Aided Design. Kuldip's research focus is in the area of Computational Fluid Dynamics and its applications. In particular Kuldip is working on multi-phase flows in pipelines and aerodynamic interventions to increase the overall fuel efficiency of commercial heavy goods road vehicles.

Taimoor Asim graduated with a degree in Mechanical Engineering from NUST (Pakistan), followed by M.Sc. in Automotive Engineering from University of Huddersfield with distinction. Afterwards he joined the University of Lahore in the Department of Technology where he worked as a Lecturer and he has completed number of projects in the development of course structure and curriculum. He headed the industrial training and placement bureau from 2009-2010. He was the group leader for the development of engineering laboratories at the University of Lahore. Currently he is a full time PhD student in the field of Computational Fluid Dynamics at the University of Huddersfield.